General Disclaimer

One or more of the Following Statements may affect this Document

- This document has been reproduced from the best copy furnished by the organizational source. It is being released in the interest of making available as much information as possible.

- This document may contain data, which exceeds the sheet parameters. It was furnished in this condition by the organizational source and is the best copy available.

- This document may contain tone-on-tone or color graphs, charts and/or pictures, which have been reproduced in black and white.

- This document is paginated as submitted by the original source.

- Portions of this document are not fully legible due to the historical nature of some of the material. However, it is the best reproduction available from the original submission.

Produced by the NASA Center for Aerospace Information (CASI)

California Institute of Technology

FINAL TECHNICAL REPORT

NASA GRANT NGR-05-002-181

MARINER 6 AND 7 PICTURE ANALYSIS

Robert B. Leighton

Principal Investigator

This report summarizes the status and results of analytical studies of Mariner 6 and 7 far-encounter (FE) pictures, carried out during the period July, 1970 to September, 1973. The purpose of the studies was to devise ways to combine digital data from the full set of FE pictures so as to improve surface resolution, distinguish clouds and haze patches from permanent surface topographic markings, deduce improved values for radius, oblateness, and spin-axis orientation, and produce a composite photographic "map" of Mars at the 1969 epoch suitable for comparison with later or earlier data.

The general status of the work at the end of the period was that the attempts to measure and correct camera distortions, locate each image in the frame, and convert image coordinates to martian surface coordinates were highly successful - residual uncertainties in location were considerably less than one pixel (picture element). However, the analysis of the data to improve the radius, figure, and axial tilt was curtailed because of the huge mass of superior data provided by the follow-on Mariner 9 spacecraft.

The procedures for superposition of successive frames to produce a composite map had been only partially worked out when the effort was suspended. All of the data, programs, and intermediate results are still available (1976) and could be carried forward with little difficulty given sufficient need and the necessary technical support.

The greater part of this report is devoted to a brief summary of the problems faced, the solutions found, and the conclusions reached in analyzing the picture data.

THE DATA

Mariner 6 returned 49 far-encounter pictures over a 2-day period, and Mariner 7 returned 92 FE pictures over a 3-day period prior to closest approach. The picture frame format comprised 700 lines having 945 pixels per line. Each pixel was represented by a digitized intensity on a scale of 0-255, called data-numbers (DN). We are not concerned here with the degree of linearity of the actual relationship between DN and intensity, but simply treat DN's as approximately linear in intensity.

The image diameters, in pixels, ranged from 145 to more than 1000, with corresponding scale factors of ~100 km/pixel to ~10 km/pixel. These scales, while far inferior to those obtained at near-encounter and by Mariner 9, are substantially

superior in resolution to earth-based pictures and thus provide valuable inter-
media!:e-resolution data. The possible importance of such data in connection
with st.dies of variable martian features prompted the program described here.

TECHNICAL OBJECTIVES

In order to derive the best possible resolution, intensity discriminability,
and geometric fidelity, it was taken as a goal to superimpose images such that
any given point on Mars, visible in a particular image, be defined within a frac-
tion - say a tenth - of a pixel. To achieve this goal entailed a considerable
analysis and correction of camera distortions, and required the invention of
highly sensitive procedures for defining the boundaries of each image. The prin-
cipal factors which entered the problem were these:

1. Camera optics. The focal length and geometrical distortions of each camera
   system had to be determined with sufficient accuracy, both for intercomparing
   the results from Mariners 6 and 7, or for combining the two data sets should
   this prove desirable.

2. Vidicon distortion. The vidicon TV sensor used in the cameras, while being
   quite satisfactorily distortion-free for ordinary purposes, did possess
   measurable distortions (of electronic origin) analogous to the optical distor-
   tions familiar in camera systems. A complicating factor here was that the
   electronic distortions were to some extent intensity-dependent.

3. Image geometry. The problem of defining the location and size of each image
   was complicated by the frequent occurrence of naze layers around the limb
   and perhaps near the terminator. The oblique view (phase angle approximately
   25°) also made it necessary to work with the relatively poorly-defined sunrise
   terminator line on half of the image rather than with a relatively sharp limb-
   sky boundary. This problem could be alleviated somewhat if one knew the focal
   length precisely and were able to assume a radius, oblateness, and distance
   for Mars. At the start of this project it was hoped that the data might yield
   improved values for the radius and oblateness, so that it was deemed necessary
   to face the image measurement problem in its most general form.

PROCEDURES

The procedures used to evaluate the system parameters, correct for aberra-
tions, and define the image shape will be discussed under the following headings:

Focal Lengths and Image Scale

Image Distortions and Their Correction

Limb Detection

Image Superposition

1. Focal Lengths and Image Scale.

The focal lengths of the cameras were defined by direct measurement in the laboratory, by viewing a calibrated illuminated reticle in the focal plane of an autocollimator using a theodolite, and then measuring the image of this reticle in the camera focal plane using a travelling microscope. (L. Adams: JPL memo of 1 July, 1969, "Narrow Angle Optics Focal Length Determination").

The present author reviewed the procedures and the data, and reduced the data using a maximum-likelihood procedure. If the various angles subtended by the cross-lines of the reticle, as viewed in the theodolite, are A_i (I = 1,2,...) and the corresponding linear positions of these lines as viewed in the focal plane are X_i (i = 1,2,...), then the focal length F may be defined in terms of these values as the best-fit value in the relation

$$(X_i - \bar{X}) = F(A_i - \bar{A})$$

where $\bar{X}$, $\bar{A}$ are the means of X_i and A_i, respectively.

The quantities X_i and A_i were both subject to uncertainties, σ_X and σ_A, which were taken into account in finding the best fit F. (Each measurement of X_i and A_i was made four times in independent runs, so that σ_X and σ_A could be evaluated: $\sigma_X = 0.003$ mm and $\sigma_A = 0.7$ arc sec.) The resulting values for F were

M6 Camera B: F = 505.44 ± .07 mm

M7 Camera B: F = 502.66 ± .07 mm

To define the linear scale of the image on the face of the vidicon, a 7 x 9 array of small, square marks was vacuum deposited through a carefully prepared mask on the inner face of each vidicon tube during manufacture. Each tube was later measured to verify the actual location of each such reseau mark. These marks were visible as black dots covering a few pixels of the image, and were not visible in unilluminated areas. Each Mars picture had at least one mark visible on it, and the later, larger images had many.

A drawing of the picture area and reseau marks is shown in Fig. 1. The reseau marks were spaced 1.8008 mm apart except for those around the edge where the spacing perpendicular to the edge was modified for frame-formatting purposes.

2. Image Distortions and Their Correction.

On the basis of uniform-illumination pictures taken during bench calibration of the systems, it was known that the recorded reseau mark locations in line-number and element-number (L,E) coordinates were not uniformly spaced but showed small, systematic departures from rectilinearity. These departures remained substantially constant throughout the tests, but varied somewhat with illumination intensity and shutter position during readout.

The first task in treating the data was thus to find the actual reseau mark locations in the flight pictures and, if sufficiently well-defined systematic behavior were found, to use the observed reseau pattern as a basis for geometric correction of the flight pictures.

All of the pictures were examined visually, the visible reseau marks were identified as to row and column (I,J), and a table of nominal (integral pixel) coordinates was made. A computer program was written which stored the local (10 x 10 pixel) neighborhood of each visible reseau mark of a picture and found the line-and element (L,E) coordinates of the darkest pixel in that neighborhood. Then, the DN values of the surrounding pixels were least-square fitted to a paraboloid of revolution

$$DN(L,E) = DNO + A*((L - XL)^2 + (E - YE)^2)$$

The fractional-pixel part of the mark location was taken as the real quantities (XL, YE) corresponding to the best fit.

The accuracy with which a given reseau mark in a given frame could be located was approximately 0.3 pixel rms, and the average over several frames was well within 0.1 pixel.

Because of a weak magnetic field associated with the spring steel shutter blade, the reseau grid was not the same for each picture. The shutter was of the flip-flop type, so that two different, but respectively constant, patterns were evident, corresponding to the two positions of the shutter during readout. These patterns differed by as much as 3 pixels at the edge of the frame, the greatest effect being a relative rotation of some 0.4 degree.

The reseau-mark-locating program thus yielded four tables of average mark locations - one for each spacecraft and shutter-blade orientation. The mark offsets varied smoothly from point to point on the vidicon target, and provided a good basis for correcting the individual picture distortions by interpolation.

Various possible schemes for utilizing the reseau shift data were considered, including a least-square polynomial fit in two-dimensions and stepwise linear, quadratic, and cubic interpolation. A bi-cubic "spline" interpolation formula seemed to have significant advantages in accuracy and economy and was the method actually used. The formulas are given in appendix A.

Using the bi-cubic interpolation formula, the pictures were transformed to a new format in which the reseau marks fell upon a precirely rectilinear grid having exactly 135 pixels between reseau marks (for those marks not lying along a picture edge). The corrected picture format had 770 lines of 935 elements each, and reseau marks fell at the element and line numbers given in Table 1. Fig. 1 shows this adopted standard reseau pattern. The curvilinear grid in this figure shows the offsets (magnified 22.5 X) of corresponding points in the original pictures. The grid lines were drawn by computer, using the bi-cubic spline interpolation scheme based upon the measured reseau mark shifts.

Table 1

Line and element numbers of Reseau Marks in corrected pictures

Row	Line	Column	Element
1	32.11	1(L mask edge)	7.29
2	120.00	2	65.00
3	?55.00	3	200.00
4	390.00	4	335.00
5	525.00	5	470.00
6	660.00	6	605.00
7	747.89	7	740.00
		8	875.00
		9(R mask edge)	932.71

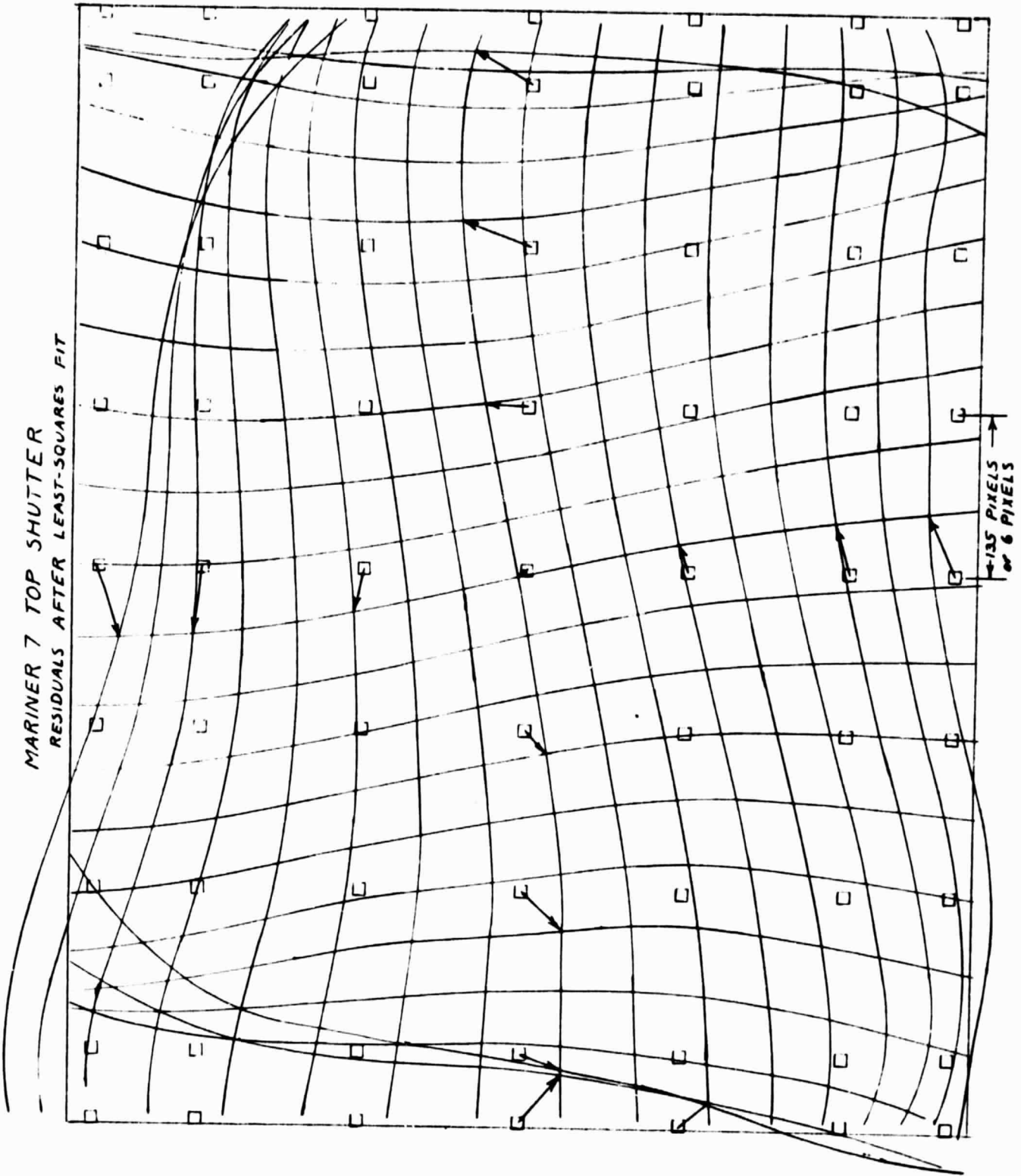MARINER 7 TOP SHUTTER
RESIDUALS AFTER LEAST-SQUARES FIT

Figure 1

The transformation was carried out as follows: For each integral pixel location (LC, EC) of the corrected picture, non-integral line-and-element coordinates $(L + \lambda, E + \epsilon)$ of the corresponding point in the "raw" picture were calculated by iteration, where $0 \leq \lambda < 1$ and $0 \leq \epsilon < 1$ are the fractional parts of the coordinates. A weighted DN value was assigned to the pixel by the formula

$$\begin{aligned} DN(LC,EC) = {} & (1 - \lambda)(1 - \epsilon)DN(L,E) \\ & + \lambda(1 - \epsilon)DN(L + 1,E) \\ & + (1 - \lambda)\epsilon DN(L,E + 1) \end{aligned}$$

This method introduces approximately one-half pixel of smearing on the average, which was considered acceptable.

The result to this point is that all pictures were transformed into a true rectilinear form, as if they had been taken by a distortion-free optical system. In the following, all references to picture coordinates are in the corrected system.

3. <u>Limb Detection</u>. The next step toward superimposability of images was to define the image location in each frame. (The spacecraft and camera platform orientations were known well enough to assure that the image would be inside the camera field, but pointing uncertainties of many pixels remained. The angular image orientation (roll) was sufficiently accurately known from space-craft data that it was not deemed necessary to determine it from the image itself.)

The easiest problem was approached first - namely, to find the sharp edge of the planet image (limb). The approximate (L,E) coordinates of the extreme boundaries of each image were estimated by eye, using pictures with (L,E) grid lines superimposed by computer. Each image edge was then mapped into eight overlapping elongated "BLOCKS", each containing about 45° of the limb or terminator. Block coordinates were (L,E) coordinates for four of the blocks and were quasi-rectangular coordinates at 45° to (L,E) coordinates for the other four. The purpose of this procedure was to permit the use of a single, simple procedure for detecting the image edge.

The principal problem was to define the "edge" of the planet in a physically resonable, operationally simple, and yet sufficiently sensitive and reproducible manner. Several criteria were devised and tested. All used

data averaged over a number of pixels "parallel" to the (computed) local
limb so as to reduce noise. Five successive lines of data were averaged,
using a suitable linear interpolation between pixels in a given line to
accommodate the local "tilt" of the image edge. Each resulting line of
data thus represented an "edge function" which ideally should start at sky-
background level, rise rapidly as the edge is crossed, and quickly level
off to the local disk intensity value inside the edge. Induced, many actual
cases showed just such behavior, but often there were also some complicating
factors: a) Haze layers, which would show an irregular rise from sky to
disk; b) the polar cap, which showed quite marked limb darkening; c) local
disk markings, which often modified or confused the ideally expected behavior.
Nevertheless, at almost all points two or more of the edge-defining criteria
would give concordant results. Fig. 2 shows examples of edge functions
taken from one image frame.

The edge functions tended to fall into four categories:

1) A sharp rise from near-zero DN values to a plateau, within a span of 4
   or 5 pixels.

2) A more gradual rise over 5-20 pixels, sometimes with an intermediate
   maximum (haze layers).

3) A steep rise for 3-4 pixels, followed by a more gradual but substantial
   further rise (polar cap).

4) A gradual, irregular rise over many pixels (terminator and north-polar
   limb region).

Several criteria were devised for locating the sharp edge characterized
by edge functions of the first type, to fractional - pixel accuracy: 1) A
correlation procedure to match the observed edge profile with that expected
on the basis of a plausible edge smearing-function was devised. A gaussian
smearing function having approximately a 2-pixel FWHM was correlated with
the first difference function of the edge function, and the (fractional-
pixel) location of the maximum of the correlation was determined. 2) A defini-
tion of the location of the planet edge in the presence of a haze layer was
the position of the innermost maximum of the correlation function used in 1)
above. This criterion was not fully refined and tested under conditions where
a clearly visible haze layer was present, and it sometimes gave wildly dis-
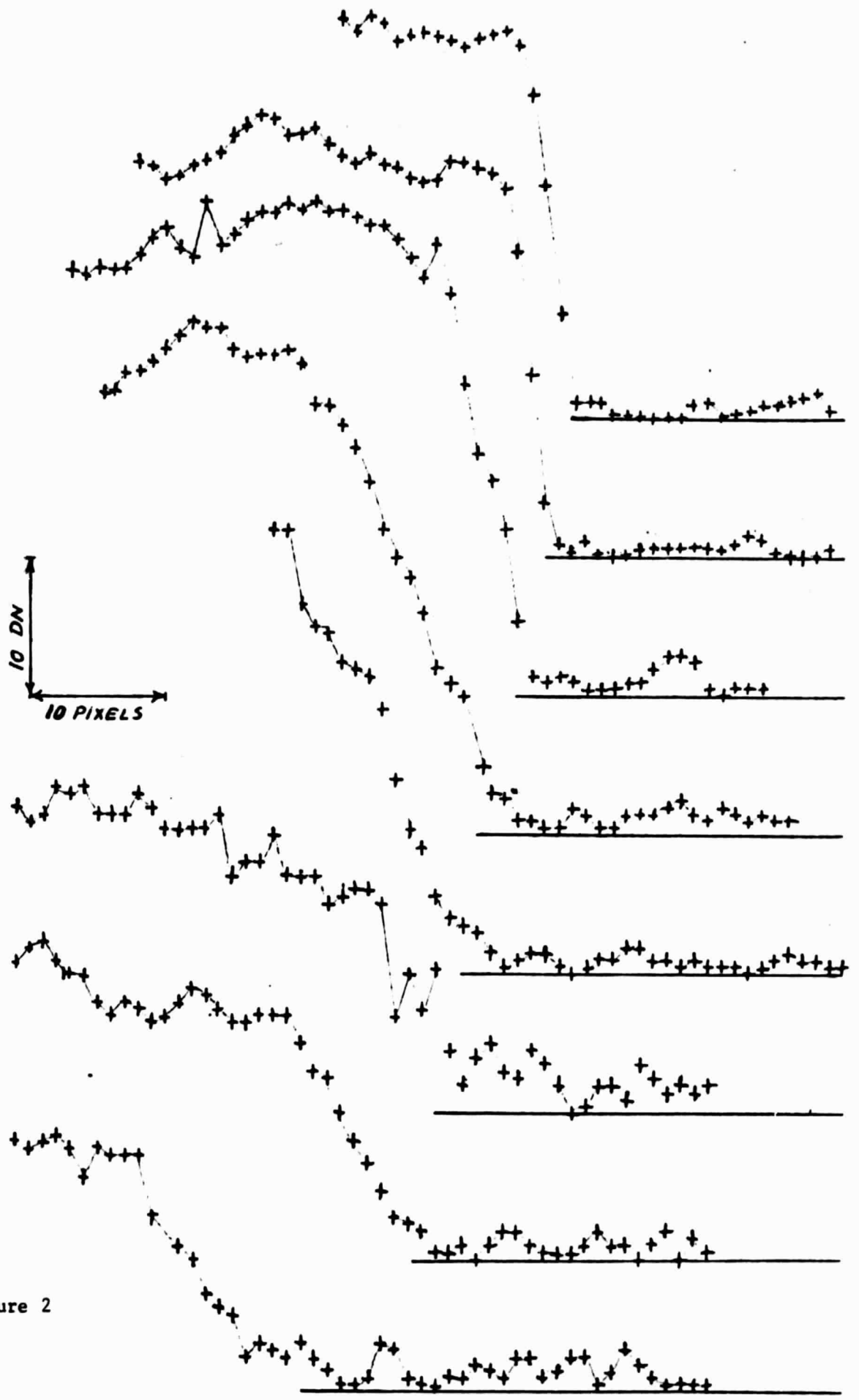cordant results in those cases where it was tried. 3) A linear least-squares

Figure 2

fit to a few consecutive points surrounding the maximum DN "jump", extra-
polated to zero and the intercept point moved toward the planet by a fixed
amount (approximately 1.25 pixel), gave another measure of the point of
maximum slope. 4) Along the terminator and in certain other areas where
it seemed appropriate, an extended linear or quadratic least-squares fit,
similar to criterion 3) above, was used. In the case of a very gradual rise,
the identification and rejection of "sky" background was a crucial part of
the procedure. The simplest way to do this was to reject all data outside
that point where any DN value was less than some threshold value.

The mutual consistency, and the sometimes systematic disagreement, of
the various edge locators is shown in Fig. 3. Over most of the span, four
out of five methods gave the same value within 0.2 pixel out of an image
radius of about 100 pixels. Systematic departures of two of the methods
are also seen, associated with the polar cap. The "gradual-rise" linear
least squares fit systematically falls outside any of the other edge values,
usually by about the expected "edge-smear" amount. All in all, the edge-
locating procedures were considered to be of excellent accuracy wherever the
edge was reasonably sharp, and of acceptable accuracy elsewhere, provided
some judgement was used in selecting among the various methods for a given
case.

4. Image Superposition.

Given suitable means of locating the bright limb and the terminator of
the planet, the coordinates of the center of the planet can be estimated. If
the full disc were illuminated, this would simply require a fit to an
ellipsoidal arc of known "tilt" in the frame. The 26° phase angle of the
solar illumination was a complication, but by use of a suitable side-
illuminated-ellipsoid model and careful assignment of relative weights to
limb and terminator data, a good fit could still be expected because of the
large number of available points and the small number of parameters.

Before it was decided to abandon the objective of finding accurate
values for the polar and equatorial radii of Mars, the question of how to
deal with systematic errors was examined. It was reasonable to believe that
the camera properties were not changing with time during the few-day far-
encounter period. The image "smear" in pixels, from all instrumental causes,
should be independent of image size. Thus a given systematic effect, related
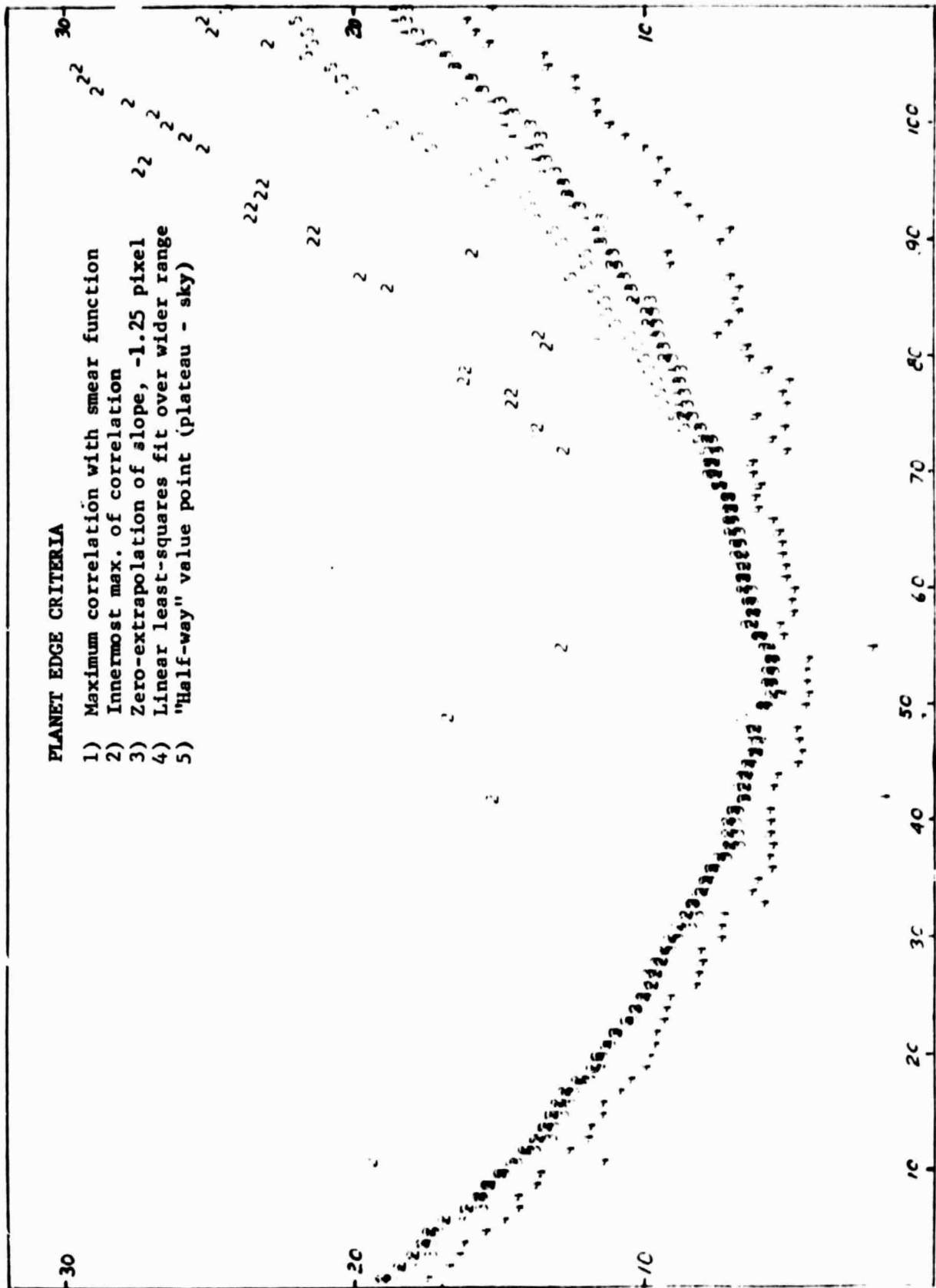
Figure 3

to the camera point-spread function, should be constant (in pixels) and
should have a greater effect on small images than on large ones. Data
from one spacecraft, analyzed in this way, did seem to show qualitatively
such an effect, but no reliable quantitative results were obtained.

Even though reliable independent radius values were not obtained, it
was still felt worthwhile to attempt a superposition of frames to yield a
quasi-mercator strip-map of the lower latitudes. Two alternative procedures
were devised. In the first, coordinates of the planet center for a given
image, deduced from a best-fit of limb and terminator data to a constant
ellipsoidal model for the Mars figure, were used to define the image point
corresponding to the ephemeris latitude and longitude of the planet center
based on spacecraft orbital and orientation data as it applied to that
image. Then, using the appropriate image scale, a matrix of standard lati-
tudes and longitudes at one of three chosen linear resolutions, was filled
with (interpolated) DN values from that image. These partial mappings were
called "strips". Two strips were formed from each image - one centered
somewhat east of the planet center, and the other an equal distance (in
longitude) west of the planet center. The purpose of the two mappings at
different local solar times was to search the resulting maps, later, for
evidences of diurual cloud, frost, haze, or other albedo effects. This
is still a good idea and could give valuable results.

The strips corresponding to a given local time, from the full set of
images, constituted an overlapping set which could be combined directly,
point by point, by simple averaging.

The second procedure, for producing a high-resolution map, started
from the strip data just discussed. However, on the assumption that the
adopted center location of each image might be slightly in error, a
procedure for improving the centering was set up: for each given strip, a
correlation function for this strip with the corresponding averaged data from
all other strips contributing to the same area was to be evaluated, and the
maximum of the correlation function was to be found by inspection as well
as by analytic means. Using the individual corrections so obtained, new
strips were to be formed from the images and the process repeated if necessary.

The above procedure was carried through to the point of producing a "raw"
strip map, which showed considerable promise. (Fig. 4) Programs to evaluate
correlations of "strip" with the "map-minus-strip" were written and debugged,

but corrected centers were not obtained.

SUMMARY

Procedures were successfully devised to combine data from separate, un-corrected pictures in a coherent way so as to produce an averaged data set having finer resolution and better signal-to-noise value than any of the original images. It was demonstrated that images can be corrected for geometric distortions; that they can be located in a frame; and that rectified strips produced from such images can be combined: all within an accuracy of from about a tenth to about half a pixel.

A POLYNOMIAL INTERPOLATION EXPRESSION FOR A

SMOOTH FUNCTION DEFINED ON A RECTANGULAR POINT GRID
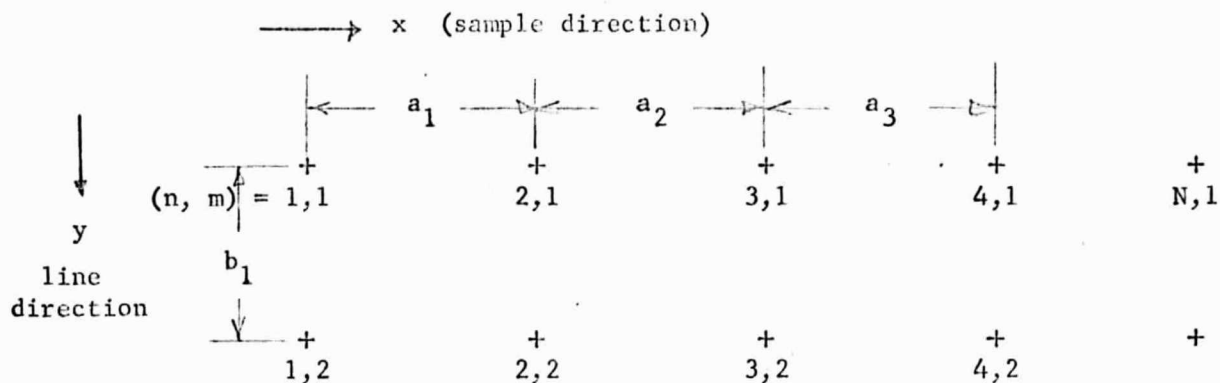
R. B. Leighton

18 July 1969

Corrected 23 March 1970, 20 February 1976

Given a rectangular grid of points whose coordinates are x_n, y_m where

$n = 1, 2, \ldots N$ and $m = 1, 2, \ldots M$

(n = sample number, m = line number)

let the x-spacing of the points be $a_r = x_{r+1} - x_r$ $r = 1, 2, \ldots N-1$

and the y-spacing be $b_s = y_{s+1} - y_s$ $s = 1, 2, \ldots M-1$.

Let $f(x,y)$ be a function whose value f_{nm} is known only at the points x_n, y_m. We wish to approximate this function by interpolation. We do this by developing a polynomial expression for $f(x,y)$ which will be used within a given rectangle whose corners are at (x_n, y_m), (x_{n+1}, y_m), (x_n, y_{m+1}), (x_{n+1}, y_{m+1}). This polynomial joins on to the corresponding expressions in neighboring domains in such a way that f and its first derivative are continuous across the boundaries.

We must first define the derivatives of f at the corner points of each rectangle. For such points interior to the array we do this by passing a parabola through three successive points. The resulting slopes are

$$f_{nm}^x = \left.\frac{\partial f}{\partial x}\right|_{\substack{x = x_n \\ y = y_m}} = \frac{a_{n-1}^2(f_{n+1,m} - f_{n,m}) + a_n^2(f_{n,m} - f_{n-1,m})}{a_n \, a_{n-1}(a_n + a_{n-1})}$$

and

$$f_{nm}^y = \left.\frac{\partial f}{\partial y}\right|_{\substack{x = x_n \\ y = y_m}} = \frac{b_{m-1}^2(f_{n,m+1} - f_{n,m}) + b_m^2(f_{n,m} - f_{n,m-1})}{b_m \, b_{m-1}(b_m + b_{m-1})}$$

Along the outermost edges of the entire grid, the derivatives perpendicular to the edge at a grid point may be defined as the slope of a parabola through the three points including the edge. (Other definitions may be used if some special symmetry is present or if there is other information.) These slopes are:

$$f_{1\,m}^x = f_{1,m}\left(-\frac{1}{a_1} - \frac{1}{a_1 + a_2}\right) + f_{2m}\left(\frac{1}{a_1} + \frac{1}{a_2}\right) + f_{3m}\left(\frac{-a_1}{a_2(a_1 + a_2)}\right)$$

$$f_{Nm}^x = f_{N-2,m}\left(\frac{a_{N-1}}{a_{N-2}\,(a_{N-2} + a_{N-1})}\right) - f_{N-1,m}\left(\frac{1}{a_{N-2}} + \frac{1}{a_{N-1}}\right)$$

$$+ f_{N,m}\left(\frac{1}{a_{N-1}} + \frac{1}{a_{N-2} + a_{N-1}}\right)$$

$$f_{n\,1}^y = f_{n,1}\left(-\frac{1}{b_1} - \frac{1}{b_1 + b_2}\right) + f_{n2}\left(\frac{1}{b_1} + \frac{1}{b_2}\right) + f_{n3}\left(\frac{-b_1}{b_2(b_1 + b_2)}\right)$$

$$f_{nM}^y = f_{n,M-2}\left(\frac{b_{M-1}}{b_{M-2}\,(b_{M-2} + b_{M-1})}\right) - f_{n,M-1}\left(\frac{1}{b_{M-2}} + \frac{1}{b_{M-1}}\right)$$

$$+ f_{n,M}\left(\frac{1}{b_{M-1}} + \frac{1}{b_{M-2} + b_{M-1}}\right)$$

With all displacements and slopes now defined, the polynomial expression

$$f(x,y) = f_{00} (1 + 2X) (1-X)^2 (1+2Y) (1-Y)^2$$

$$+ f_{01} (1+2X) (1-X)^2 Y^2 (3-2Y)$$

$$+ f_{10} X^2 (3-2X) (1+2Y) (1-Y)^2$$

$$+ f_{11} X^2 (3-2X) Y^2 (3-2Y)$$

$$+ a_n f_{00}^x X(1-X)^2 (1+2Y) (1-Y)^2$$

$$+ a_n f_{01}^x X(1-X)^2 Y^2 (3-2Y)$$

$$- a_n f_{10}^x X^2(1-X) (1+2Y) (1-Y)^2$$

$$- a_n f_{11}^x X^2(1-X) Y^2 (3-2Y)$$

$$+ b_m f_{00}^y (1+2X) (1-X)^2 Y (1-Y)^2$$

$$- b_m f_{01}^y (1+2X) (1-X)^2 Y^2 (1-Y)$$

$$+ b_m f_{10}^y X^2 (3-2X) Y (1-Y)^2$$

$$- b_m f_{11}^y X^2 (3-2X) Y^2 (1-Y)$$

meets the desired conditions, where

$$f_{00} = f_{nm}, \quad f_{01} = f_{n, m+1} \quad \text{etc.}$$

and
$$X = \frac{x-x_n}{a_n} , \quad Y = \frac{y - y_m}{b_m}$$